Int. J. Electrochem. Sci., 10 **(2015)** 2141 - 2154

International Journal of
ELECTROCHEMICAL
SCIENCE
www.electrochemsci.org

Corrosion study of Fe-Al Intermetallic Alloys in Simulated Acid Rain

E. Huape-Padilla[1,2], M. Sánchez-Carrillo[1], J.P. Flores-de los Rios[1], M.A. Espinosa-Medina[2], R.G. Bautista-Margulis[3], M. I. Ferrer-Sánchez[3], G. Carbajal-de la Torre[2], L. Bejar-Gómez[2], J. G. Chacón-Nava[1], A. Martínez-Villafañe[1,]*

[1] Centro de Investigación en Materiales Avanzados (CIMAV), Departamento de Metalurgia e Estructural, Laboratorio de Corrosión, Miguel de Cervantes No. 120, 31109 Chihuahua, Chih., Mexico.
[2]Facultad de Ingeniería Mecánica, UMSNH, Santiago Tapia 403 Col. Centro, C.P. 58000 Morelia, Michoacán, Mexico.
[3] División Académica de Ciencias Biológicas, Universidad Juárez Autónoma de Tabasco, C.P. 86040, Villahermosa, Tabasco, México.
[*]E-mail: martinez.villafane@cimav.edu.mx

Received: 7 November 2014 / *Accepted:* 28 December 2014 / *Published:* 19 January 2015

This paper presents an investigation on the corrosion resistance of iron aluminides FeAl-based alloys, in an environment that simulates acid rain water in temperature room. Potentiodynamic Polarization, Linear polarization resistance curves Rp, Nyquist data and Bode curves obtained by electrochemical impedance spectroscopy were used to study the corrosion behavior of two intermetallic compounds. Showed that the binary alloy FeAl exhibited the greatest resistance to corrosion while the alloy Fe_3Al showed the lowest resistance to corrosion. Intermetallic Fe_3Al alloys had greater susceptibility to pitting corrosion. While FeAl intermetallic alloys showed low corrosion rate.

Keywords: Corrosion, iron aluminides, acid rain, electrochemical techniques.

1. INTRODUCTION

Iron aluminides, mainly based in the stoichiometric compositions of Fe_3Al and FeAl, have a great potential in a variety of structural application such as automobile and aero-space industry in substitution of superalloys, since they offer excellent resistance to oxidation and sulphidation in high temperature, with low material cost and density [1, 2]. Due to technical and environmental reasons, a great deal of effort has been done in order to get a better understanding about the corrosion behavior. Corrosion behavior of iron aluminides such as Fe_3Al and FeAl has been investigated in an environment

that simulates human body fluids (Hank's solutions) as biomaterials [3, 4]. Another application of iron aluminides where corrosion behavior has been investigated as structural materials in the construction of boiler or supercritical steam turbines, exposed to temperatures between 600°C and 700°C in corrosive environments such as molten salts, molten-salt corrosion is very similar to aqueous corrosion [5]. Similarly, iron aluminides have been studied in high temperature corrosion in atmospheres of N_2 +SO_2 as well as Na_2SO_4–V_2O_5 molten salts and molten (Li + K) carbonate [6-8].

As structural materials such as turbines or airframes, iron aluminides are prone to be attacked in atmospheric corrosion in urban and coastal areas, industrial and marine environments corrosion are more aggressively due to the highly corrosive nature of air pollutants [9]. Nowadays, the chemistry of precipitation has been widely investigated in many countries, which are significantly affected by acid rain. The acid rain is primarily caused by the precursors of strong acids such as H_2SO_4 and HNO_3, resulting from fossil fuel combustion [10]. Countries like Mexico where human activities have an important effect on global and regional environment, has a variation in pH values of rain water. Given that Mexico City is one of the most polluted cities in the world, due to industrial activity and the large number of vehicles, air pollution of the city has received primary attention, the pH value of acid rain reported have been 4.11 [11]. Similarly in coastal areas where chemical composition of rainwater varies, pH of acid rain has been investigated in the Gulf of Mexico, showing that rain acidity is higher, previous results in rain water at the Yucatan Peninsula showed that NO_3^- levels were almost four times higher, indicating a notable enrichment of nitrate, it was strongly supported by the fact that the lower pH value 3.48 was measured [12]. Other areas such as Acapulco, Cancun, Tapachula, Tropical Pacific Ocean and Campeche, pH values of 5.96, 6.14, 5.28, 5.56 and 4.64 respectively have been reported [13, 14].

The purpose of the present research work was to evaluate the corrosion behaviors of Fe_3Al and FeAl alloys in simulated acid rain by using the electrochemical techniques and thus establishing the involved mechanisms in the process.

2. EXPERIMENTAL METHODS

2.1 Materials

Table 1. Chemical composition of the tested alloys.

Samples	Alloy Composition			
	(wt.%)		(at.%)	
	Fe	Al	Fe	Al
FeAl	71.98	28.02	55.38	44.62
Fe_3Al	82.35	17.65	69.27	30.73

The alloys used in this work (Table 1) were produced as round 20 g buttons with 99.99% pure Al, 99.97% pure Fe, on a water-cooled copper crucible under an Ar atmosphere. The buttons were

remelted at least 8 times to ensure sufficient homogeneity. Chemical composition was determined by SEM-EDX (field emission, JSM-7401F). The phase composition of the alloys was determined by the XRD method with a PANalytical diffractometer using CuKα radiation. The data identification was carried out using the Match program.

2.2 Sample preparation

Specimens were prepared by encapsulation in fast cure acrylic which, in turn, was performed by grinding the specimens from 180 to 4000 grit paper.

2.3 Electrochemical techniques

In order to simulate the acid rain conditions, the chemical composition for this environment for in vitro corrosion studies of pH 2.3, is given in Table 2. It was prepared with distilled water and analytical grade reagents following previously-reported concentrations [15].

Electrochemical tests were performed using an ACM Instruments potentiostat controlled by a computer. All potentials were measured using a Saturated Calomel Electrode (SCE) as reference electrode and a graphite bar counter electrode. All tests were performed at room temperature. The volume of electrolytic solution into the cell was 60 ml. The electrochemical techniques included potentiodynamic polarization curves, linear polarization resistance (LPR) and electrochemical impedance spectroscopy (EIS) measurements. Corrosion rates were calculated in terms of the corrosion current, i_{corr}, by using linear polarization resistance curves.

Potentiodynamic polarization curves were obtained by varying the applied potential with respect to the open circuit potential (OCP), from -500 mV up to +1500 mV at a scan rate of 1 mV/s in accord with ASTM G3-89. A delay time of 60 min was setup until a stable reading was achieved, after that, electrochemical tests started. EIS tests were carried out by using a signal with amplitude of 20 mV vs. the OCP between a frequency interval of 0.05 Hz to 10 kHz obtaining a measurement at 30 min, 12 and 24 hours of immersion. Measurements of LPR were performed by polarizing the specimen from +15 to -15 mV vs. OCP at a scan rate of 1 mV/s each 15 minutes during 24 hours. Corrosion products analysis of as-cast corroded samples was realized by scanning electron microscope (SEM) and energy X-ray dispersed spectroscopy (EDS).

Table 2. Concentrations of simulated acid rain solution.

Component	Concentration
Sulphuric acid	0.06 $ml \cdot L^{-1}$
Nitric acid	0.02 $ml \cdot L^{-1}$
Sodium nitrate	0.0265 $g \cdot L^{-1}$
Ammonium sulfate	0.0462 $g \cdot L^{-1}$
Sodium sulfate	0.0345 $g \cdot L^{-1}$
Sodium chloride	0.0875 $g \cdot L^{-1}$

3. RESULTS AND DISCUSSION

3.1. Microestructural characterization

The as-cast microstructures of the Fe_3Al and FeAl alloys are shown in Fig.1a and Fig.1b respectively. As show in Fig.1a, Fe_3Al alloy has an equiaxed grain morphology with a grain size bigger than 500 μm with a presence of pores. No precipitates were observed in this intermetallic alloy, confirmed by X-ray diffraction pattern, where crystal structure corresponding to Fe_3Al alloy without presence of second phases, see Fig.2b. In Fig.1b, FeAl alloy is composed of elongated and equiaxed grain with average size around to 100-300 μm, with presence of pores. X-ray diffraction pattern of FeAl intermetallic alloy, confirmed that crystal structure corresponding to FeAl without presence of second phases and precipitates, as can be seen in Fig.2a.

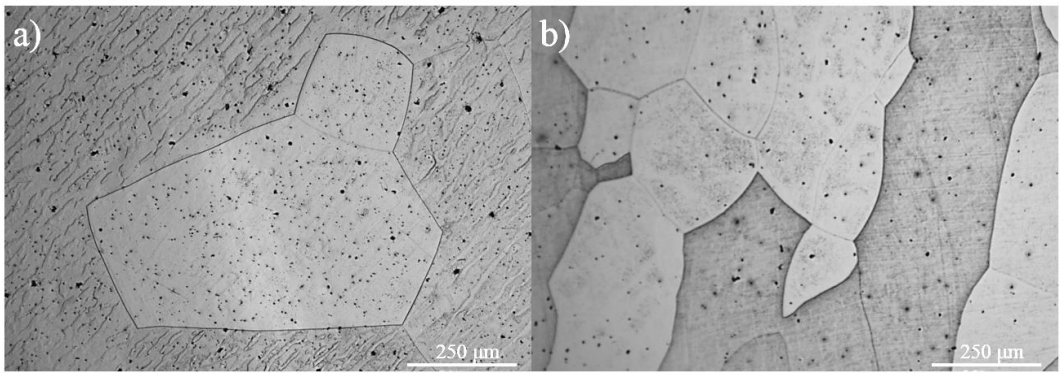

Figure 1. Micrograph of the as-received state sample a) Fe_3Al and b) FeAl.

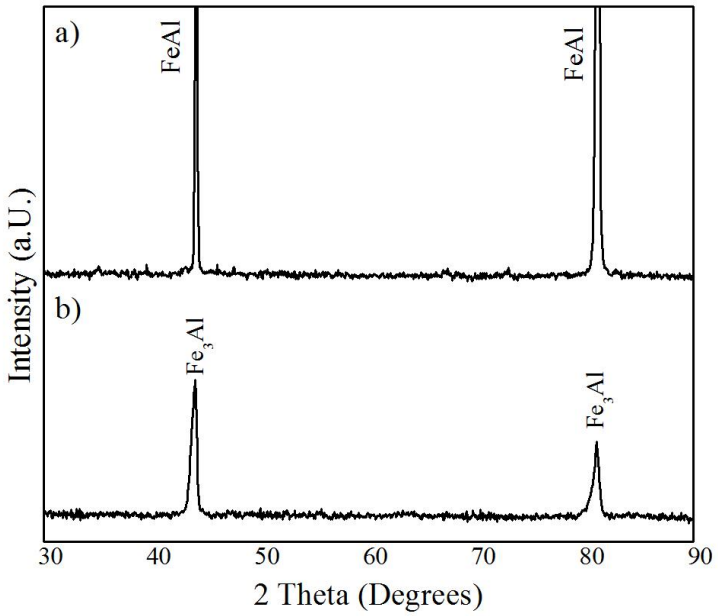

Figure 2. X-ray diffraction patterns of the as-cast condition sample of a) FeAl and b) Fe_3Al system alloys.

3.2. Potentiodynamic Polarization Curves

Potentiodynamic polarization test were realized after the initial corrosion potential reached a stable value, having approximately 15 minutes delay. Figure 3 shows the potentiodynamic polarization curves for the two alloys. Table 3 summarizes the corrosion potential (E_{corr}) and corrosion current density (i_{corr}) values obtained by intercept method, the Tafel slopes were determined by linear fitting of the potentiodynamic polarization data in the range of ±150mV of the Ecorr, in Fe3Al alloy can see that the reaction rate is slightly faster therefore the cathodic process is controlled by concentration polarization, with the current increase, the reaction rate is slow resulting in activation polarization.

Polarization (fig.3) results showed that the alloy Fe3Al presented a behavior slightly more nobly with regards to the FeAl alloy (table1). Potentiodynamic results in the Anodic region indicated that the intermetallic Fe3Al presents an active region of Anodic dissolution in a range - 767 and - 697 mV, followed by a passive behavior in the potential range - 697 mV to - 625 mV. Similarly, the intermetallic FeAl showed an active region of dissolution potential of - 802 to - 714 mV range, followed by a passive behavior in the range of - 714 mV to - 666 mV. Both materials have a behavior of Anodic dissolution after the behavior described above, during the increase in overpotencial of around 150 mV, followed semi-passive behavior and current limit with fluctuations of current density over a range of 200 mV approximately similar to those observed in materials that have corrosion pitting [16]. With the increase of the overpotencial, the behavior of the materials was active.

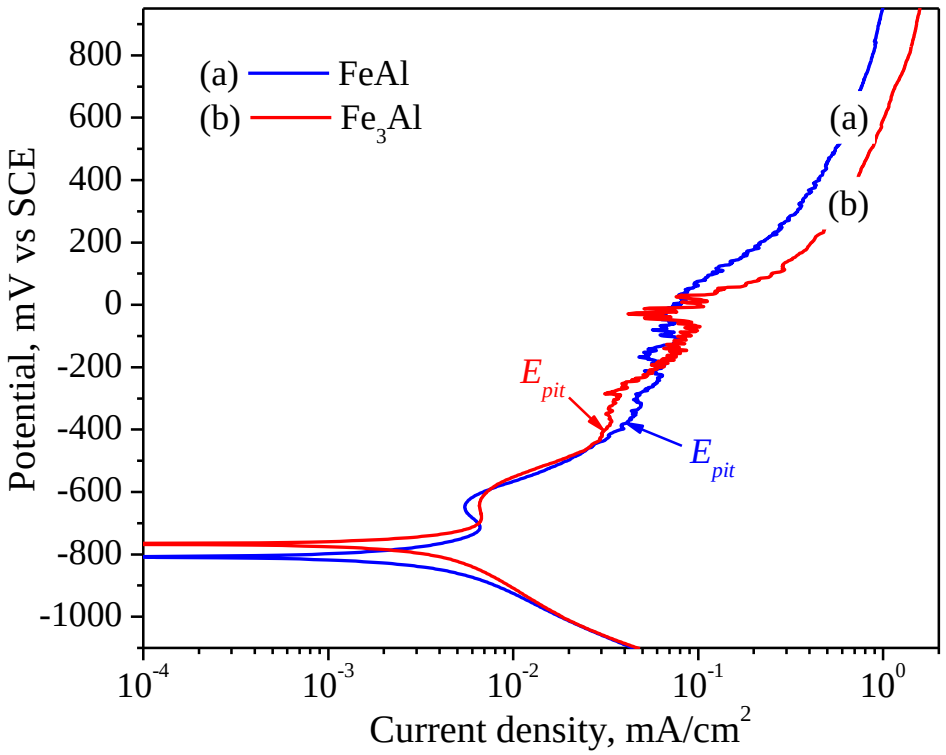

Figure 3. Potentiodynamic polarization plots of Fe_3Al and FeAl as-cast condition in acid rain electrolyte.

Table 3. Electrochemical parameters obtained from polarization plots.

Alloy	B_a (mV/decade)	B_c (mV/decade)	E_{corr} (mV)	I_{corr} (mA/cm^2)	E_{pit} (mV)
FeAl	89	100	-807	0,001463	-422
Fe_3Al	78	106	-767	0,001674	-447

3.3. Long term tests

The results of materials evaluation on acid rain intermetallic LPR are shown through the kinetics of corrosion rate and potential. Figure 4 shows the results of the variation of the potential of corrosion Ecorr with respect to time. Fe_3Al intermetallic alloy presented a decline in the value of Ecorr within 8 hours from mV - 660 to - 725, subsequently stabilizing around this last value; while the FeAl presented a gradual decline in the value of mV - 690 to - 740 Ecorr during the first 12 hours approximately, keeping it in the form fluctuated around this last value (fig. 4). There is an increase in the activity for both materials by the interaction of the rain acidic components, promoting the localized dissolution of high energy sites, such as microstructure, pores and edges of grain defects were observed on the characterization of the material arrival, Figure 1 [17]. Subsequently, Ecorr value is stabilized for both materials, which is related to a form of more homogenous corrosion, including the surface of localized corrosion sites. Figure 5 presents the images of the corroded surface of intermetallic materials, where are the sites of localized corrosion associated with microstructural defects and an adjacent area with minimal degradation, similar to that reported by Szklarska-Smialowska [18]. The analysis of corrosion products found on the surface indicated the formation of a mixture of aluminum oxide and sulfate of iron, as shown in Figure 6 which shows the chemical analysis by EDS of alloy Fe3Al (point 1).

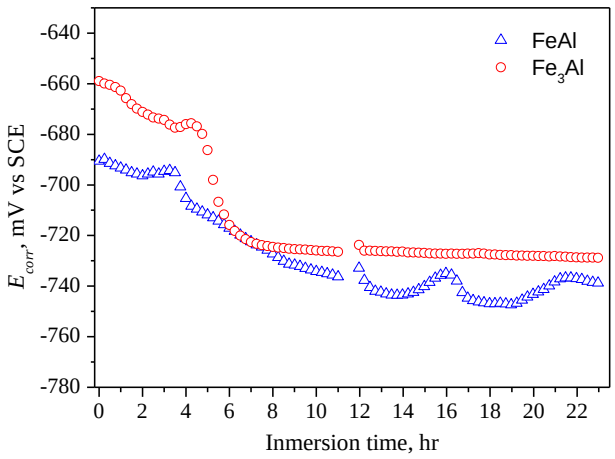

Figure 4. E_{corr} diagram of Fe_3Al and FeAl Intermetallics alloys.

The electrochemical reactions are given during the dissolution active, in an acid medium, and the intermetallic alloys FeAl base.

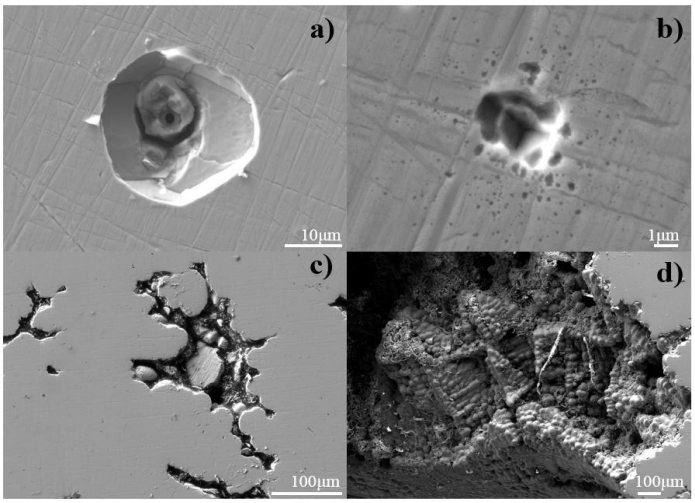

Figure 5. SEM micrograph of the corroded surfaces in simulated acid rain as cast condition of a) and b) Fe3Al, c) and d) FeAl.

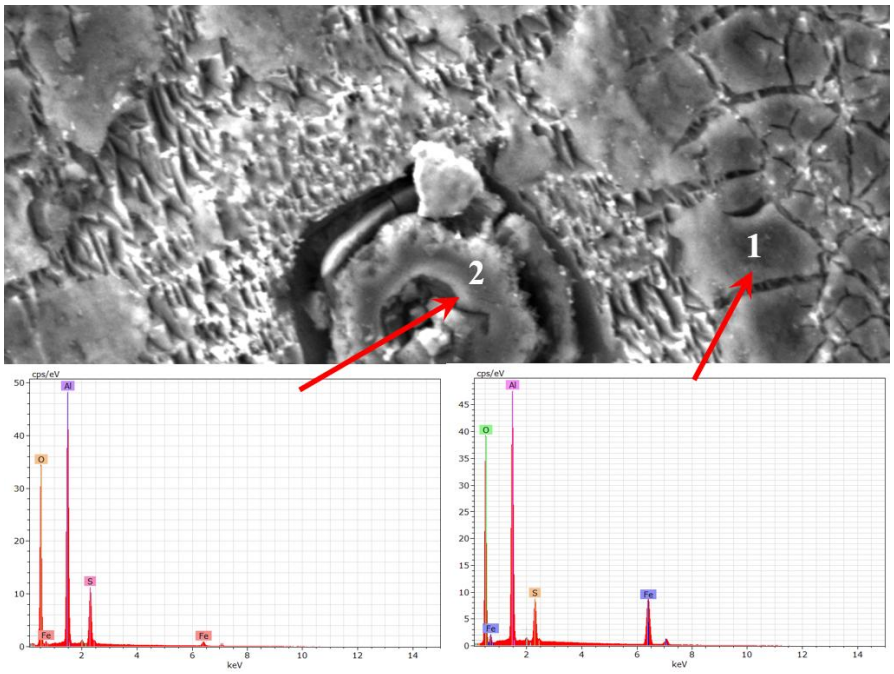

Figure 6. Photomicrographs of a pitting zone of Fe_3Al with formation of corrosion products in simulated acid rain.

During the active dissolution, in an acid medium, the intermetallic alloys base FeAl, presented the following reactions:

$FeAl + 6H^+ = Fe^{3+} + Al^{3+} + 3H_2$

$Fe_3Al + 6H^+ = 3Fe^{3+} + Al^{3+} + 3H_2 + 6e^-$

$Fe_3Al + 6H^+ = 3Fe^{2+} + Al^{3+} + 3H_2 + 3e^-$

These reactions are balanced by the reaction that occurs below, which consumes electrons:

$2H_2O + 2e^- = H_2 + 2OH^-$

The presence of the H_2SO_4 involves the formation of a ferrous sulphate:

$3Fe^{2+} + 3H_2SO_4 = 3FeSO_4 + 3H_2O$

Since the mobility of the Al^{3+} is low compared to the Fe ions within the protective film, after the area of active dissolution, aluminum rapidly becomes porous Al_2O_3 on the surface of the protective film, by the following reaction:

$2Al^{3+} + 3H_2O = Al_2O_3 + 6H^-$

From the results of linear polarization (LPR) resistance, the corrosion rate of kinetics was calculated (see Figure 7) according to the standard ASTM G102, where the corrosion rate is expressed as Equation 1:

$$CR = K\frac{i_{corr}}{\rho}EW \quad (1)$$

Where EW = is the equivalent weight of alloy, icorr Portland is the corrosion current density, ρ = density of the alloy, and K = constant. The equivalent weight was calculated with equations 2 and 3.

$$EW = \frac{\mathbf{1}}{Q} \quad (2)$$

$$Q = \sum \frac{n_i f_i}{W_i} \quad (3)$$

Where fi = the fraction of mass of the element i-th in the alloy, Wi = atomic weight of the i-th element in the alloy and ni = the valence of the i-th element of the alloy. The corrosion current density was calculated from measurements of the polarization resistance, as follows:

$$i_{cor} = \frac{B}{Rp} \quad (4)$$

Where B = constant Stern-Geary, which was obtained with the pending anodic and cathodic of Tafel, with the following equation:

$$B = \frac{\beta_a \beta_c}{2.303(\beta_a + \beta_c)} \quad (5)$$

Figure 7 shows the kinetics of corrosion obtained from the LPR calculations. The intermetallic Fe_3Al presented a decline in the value of Ecorr within 8 hours from - 660 to - 725 mV approximately. In Figure 7, the kinetics of CR of both samples was evidenced. The results showed that the present values of both alloys sustained the corrosion rate in the first 5 hours of immersion, around 80 and 88 µm/year for the FeAl to Fe_3Al respectively (fig. 7), being the FeAl material with lower values of CR, however, their CR increased continuously up to maximum values of CR around 110 µm/year presenting fluctuations of these values in the range of 11 to 24 hours of immersion. In counterpart, FeAl alloy showed a fast increase of RC after 5 hours and within 3 hours of immersion reaching CR values around 110 µm/year (similar to the highest obtained by the Fe_3Al), remaining in this range for the rest of the test (fig. 7).

Similarly to the behavior of the electrochemical potential (fig.4), during the first hours of immersion activity remained stable, suggesting a material surface homogeneously and describing a first stage of semi-passivation (fig.3) or limitation in the electrochemical activity, which is broken by the increase in activity associated with a difference of chemical concentration and the presence of

microstructural defects that promote localized first layer solution formed [19, 20]. With these events, the potential and current density is increased, presenting passivation and breaking of the formed layer events early in the localized sites (fig.5) resulting in an increase and fluctuation of the values of CR (fig.7). Although the kinetics of corrosion increased over time, it remained lower than those reported by Shankar Rao [21] who reported that FeAl alloys that contain percentages of the elderly to the 15-20 at.%, have low corrosion rates.

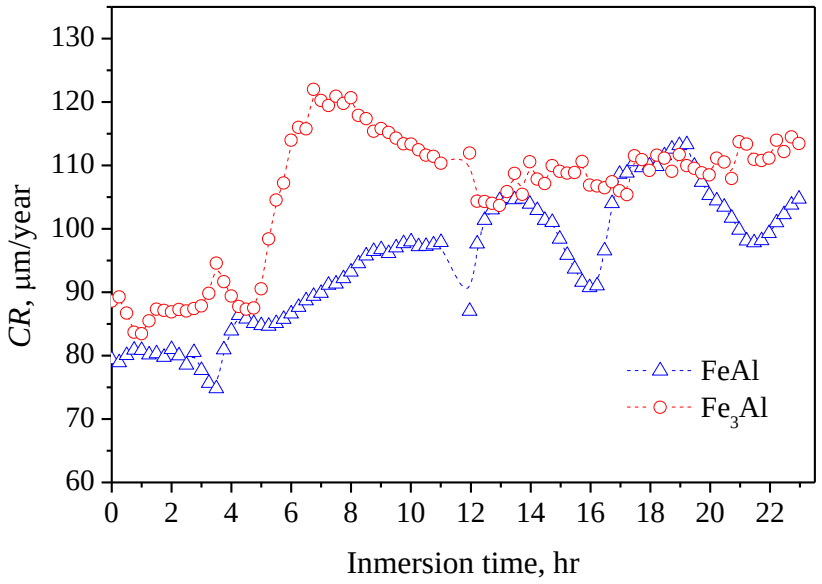

Figure 7. Corrosion rate kinetics of corroded Fe-Al intermetallics immersed in simulated acid rain solution.

3.4. EIS tests.

Figures 8 and 9 show the behavior of the two materials in the solution of acid rain, exhibiting capacitive behaviors from the Highlands of frequency to midrange, whose magnitude increased with the immersion time. At the beginning of the dive (within 30 minutes) both alloys presented a decline semicircle between the high frequencies and half associated activation behavior, followed by a resistive behavior at low frequencies (fig.8a and 9A), associated with processes of mass transport by diffusion, effect of the seudo-passiva layer, the current limit, and the adsorption of species in localized corrosion [22] sites. The results of EIS displayed at 12 and 24 hours of immersion presented a modification in the initial behavior for both alloys. In this regard, the EIS results of the intermetallic Fe_3Al at 12 hours of immersion showed a resistive behavior followed by a capacitive behavior at high frequencies and middle respectively, the latter describing a loop to the 10 Hz and 21 ° (fig.8b). Similarly to the 24 hours of immersion, it described a resistive and capacitive high frequency behavior and socks (with a loop at the 10 Hz and 25 °, fig.8b) respectively. At 12 and 24 hours of immersion, both alloys were defined semicircles indicating that they were controlled mainly by an activation process with an inductive influence on the sites of sting and a diffusion effect in the rest of the surface.

Alloy Fe_3Al at 12 h of immersion also presented this inductive loop at low frequencies, associated to the decrease in concentration of intermediate species adsorbed on the surface [23]. At 24 hours of immersion, the main control was due to activation at intermediate frequencies, with a finite diffusion response or current limit at low frequencies.

Similar to that offered by the intermetallic Fe_3Al, at 12 and 24 hours of immersion, the FeAl showed a resistive behavior followed by a capacitive behavior at high frequencies and middle respectively, the latter describing a loop to the frequencies of 7.5 Hz and 29 ° and 8.0 Hz and 31 ° for 12 to 24 hours of immersion respectively (9B) times. At low frequencies to these times of immersion, presented by this intermetallic behavior is similar, described an inductive and diffusive behavior associated with the response of the areas of localized corrosion and uniform corrosion of the areas of the intermetallic surface (fig. 5). FeAl alloy results showed a change in the size and shape of diagrams, the capacitive arches increased due to an increase in resistance to the polarization [23], showing better performance in this environment as described in the kinetics of CR (fig.7).

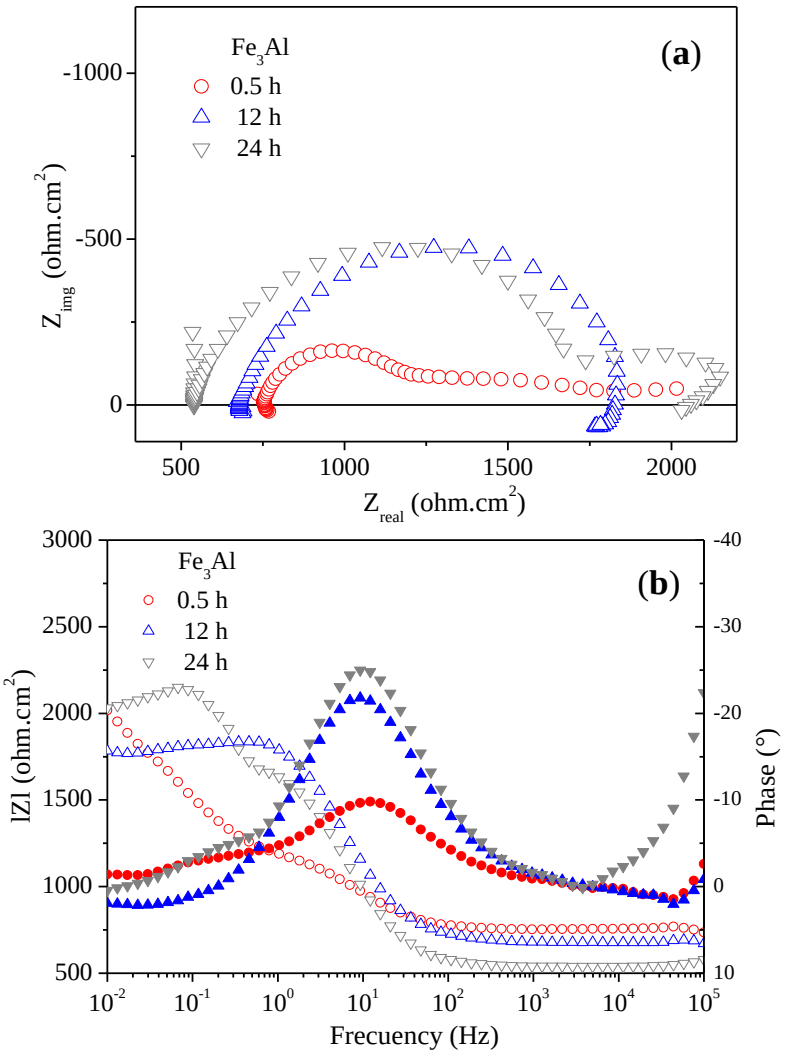

Figure 8. Electrochemistry impedance spectroscopy response for Fe_3Al, a) Nyquist and b) Bode plots.

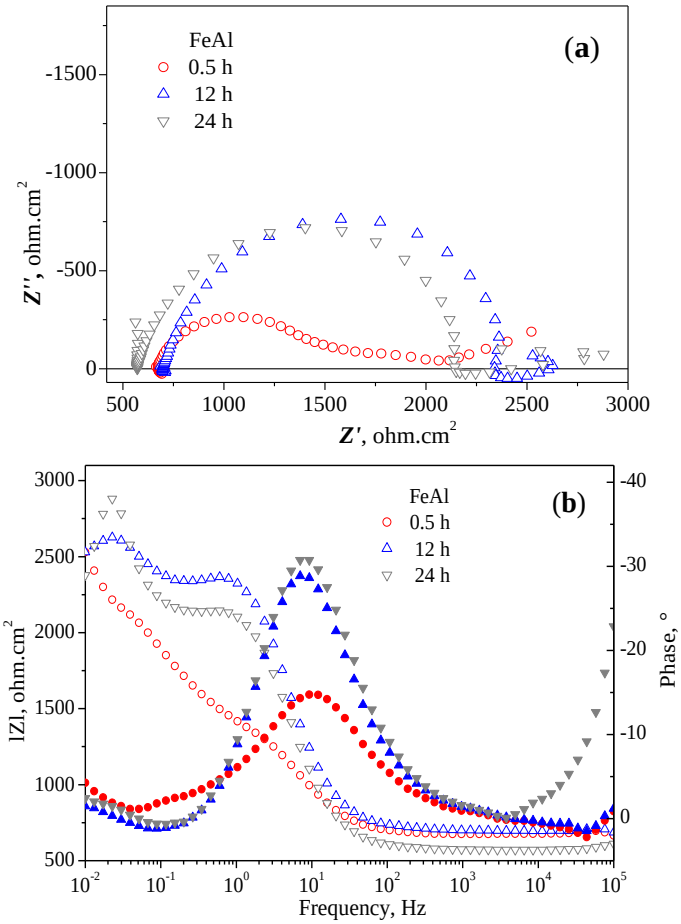

Figure 9. Electrochemistry impedance spectroscopy response for FeAl, a) Nyquist and b) Bode plots.

According to the results of the EIS and the morphological and chemical characterization by SEM and EDS of corroded samples shown in figures 8, 9 and 5, the behavior of intermetallic materials surface associated with capacitive behaviors to the midrange and inductive diffusion behavior and low frequencies, was associated with the observed surface forms of corrosion. (Figure 5a) and 5b) showed the micrographs of two areas of alloy Fe_3Al corroded after 24 hours of immersion in simulated acid rain solution, showing corrosion pitting similar to that reported previously [5.24]. The iron aluminides have high susceptibility to corrosion pitting in media with contents of C^- [25], however, a minimum of 6 X 10-4 M CL concentration - is necessary for this type of corrosion be present in the [26] iron aluminides. In this investigation, the concentration was 1.5x10-3 M Cl-, which is slightly more than the minimum reported concentration. According to the results of the electrochemical evaluations, it is suggested that the pitting originates from the beginning of the corrosion phenomenon, governed by an activation process to the initial state, followed by a mechanism of diffusion and adsorption in the interphase or intermediate reactions in the double layer inductive [27]. Figures 5c and 5d, shows the micrographs at different magnifications of the surface alloy for the FeAl corroded after 24 hours. At this point corrosion pitting was observed and attributed to the effect of the microstructure, as reported by Kim and Buchanan [21] who evaluated the effect of the change of microstructure (DO3 and B2) in corrosion behavior, determining that the B2 (FeAl) structure presented best performance in media with

contents of Cl-. Likewise it has been reported that the iron aluminides have good resistance to corrosion pitting in the presence of sulfates [21], however, does not apply with the presence of Cl-. Sulfates promote initiation of pitting of iron due to the formation of a passive iron sulfate layer, while the aluminum does present it. This may suggest that sulfate retards the oxidation of Fe^{3+} or sulfate anion adsorption to promote the reduction of species of Fe^{2+} in the interface. Thus, an increase in the dissolution of the alloy is promoted during the first stage of the [26] iron aluminide passivation, as illustrated in Figure 5d. In acid media the presence of NO^{3-} does not affect directly the corrosion process, since it only has a corrosive effect on basic media [28]. Figure 10 shows a SEM micrograph of a film after immersion for 24 hours of the intermetallic Fe_3Al under OCP conditions, which presents the chemical elemental analysis or chemical mapping by identifying the density of concentration of the Al, Fe, and S. In acidic electrolytes, the presence of Al in the film is present in small quantities due to the better [29] aluminum oxide solubility. The composition of passive films formed in FeAl alloy in sulfuric acid are dominated by significant amounts of a phase of aluminum mixed with lesser amounts of iron oxide oxy-hydroxide located at the top of the movies [2]. According to the EDS analysis of item 2 in Figure 6, the reduction process of faith in the product formed in the alloy Fe_3Al sting, can be given by the following reaction of hydrolysis:

$Fe^{2+} + 2Cl^- = FeCl_2 + 2e^-$

$FeCl_2 + 2H_2O = Fe(OH)_2 + 2H^+ + Cl^-$

FeCl2 + 2H2O = Fe (OH) 2 + 2 H + + Cl - the Cl - generated, react again with Fe2 + present in the protective film.

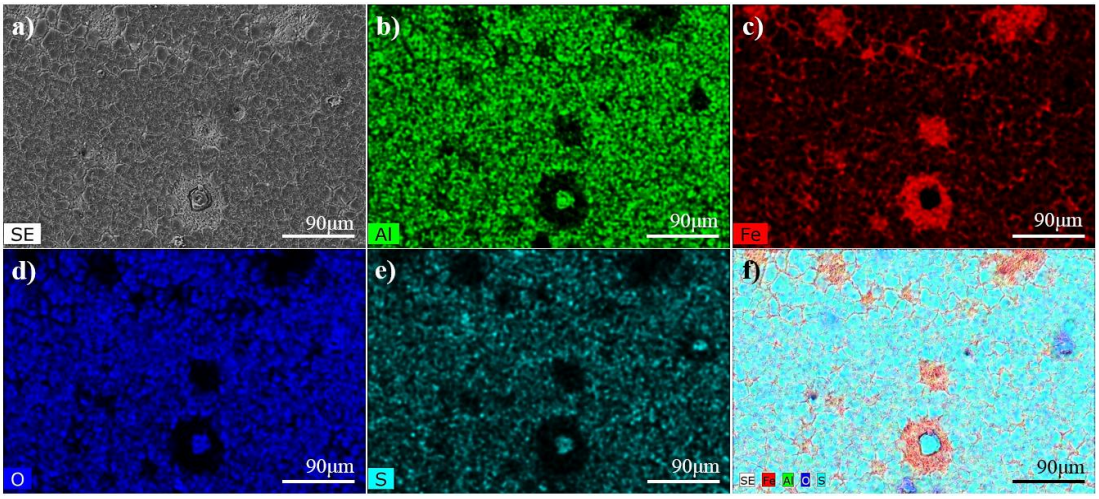

Figure 10. Photomicrographs of a) Fe_3Al corroded in simulated acid rain at 23°C, with X-ray mappings of b) Al, c) Fe, d) O, e) S and f) all elements.

4. CONCLUSIONS

The corrosion behavior of FeAl based intermetallic alloys as aircraft components to be used in acid rain environment have been evaluated. The unfavorable effect of Cl- was the main factor affecting the pitting corrosion behavior in a medium with simulated acid rain, while the presence of S promoted

the formation of a passive iron sulfate layer in Fe_3Al. The presence of NO^{3-} did not affect directly the corrosion process. Pitting resistance of Fe_3Al intermetallic alloys compared to FeAl showed a greater susceptibility to pitting corrosion. Corrosion rates of FeAl and Fe_3Al base alloys showed that the FeAl material presented lower values of CR, however, their CR increased continuously as a function of exposure time. FeAl-base alloys were found to be very promising for airline applications with their corrosion resistance.

ACKNOWLEDGEMENTS
E. Huape-Padilla thanks to the CONACYT of the grant to carry out his doctoral studies.

References

1. W.C. Luu and J.K. Wu. *Corrosion Science*, 43 (2001) 2325.
2. S. Frangini, N.B. De Cristofaro, A. Mignone, J. Lascovich and R. Giorgi. *Corrosion Science*, 39 (1997) 1431.
3. R.A. Rodríguez-Díaz, J. Uruchurtu-Chavarín, A. Molina-Ocampo, J. Porcayo-Calderón, M. González-Pérez, J.M. López-Oglesby, J.G. Gonzalez-Rodríguez and J. A. Juárez-Islas, *Int. J. Electrochem. Sci*, 8 (2013) 958.
4. C.D Arrieta-Gonzalez, J. Porcayo-Calderón, V.M. Salinas-Bravo, J.G. Gonzalez-Rodriguez and J.G. Chacon-Nava, *Int. J. Electrochem. Sci*, 6 (2011) 4016.
5. M.A. Espinosa-Medina, G. Carbajal-De la Torre, H.B. Liu, A. Martínez-Villafañe and J.G. González-Rodriguez, *Corrosion Science*, 51 (2009) 1420-1427.
6. M.A. Espinosa-Medina, H.B. Liu, G. Canizal and J.A. Ascencio, *Materials Science and Engineering* A, 443 (2007) 87.
7. J.G. Gonzalez-Rodriguez, S. Haro, A. Martinez-Villafañe, V.M. Salinas-Bravo and J. Porcayo-Calderon, *Materials Science and Engineering* A, 435 (2006) 258.
8. J.G. González-Rodríguez, A. Luna-Ramírez, M. Salazar, J. Porcayo-Calderon, G. Rosas and A. Martínez-Villafañe, *Materials Science and Engineering* A, 399 (2005) 344.
9. L. Yang, Y. Zhang, X. Zeng and Z. Song, *Corrosion Science*, 59 (2012) 229.
10. H. Wang and G. Han, *Atmospheric Research*, 99 (2011) 190.
11. A. Báez, R. Belmont, R. García, H. Padilla and M.C. Torres, *Atmospheric Research*, 86 (2007) 61.
12. R.M.B. Cerón, H.G. Padilla, R.D. Belmont, M.C.B. Torres, R.M. García and A.P. Báez, *Atmospheric Environment*, 36 (2002) 2367.
13. R.M. Cerón, A.V. Córdova, J. Zavala and M. Muriel, *Global NEST Journal*, 7 (2005) 212.
14. R.M. Cerón,, M. Muriel and B. Cárdenas, *Global NEST Journal*, 10 (2008) 92.
15. L. Feng, S. Ying-wei, S. Da-yong and H. En-hou, *Trans. Nonferrous Met. Soc. China*, 20 (2010) 638.
16. Woo-Jin Lee and Su-Il Pyun. *Electrochimica Acta*, 45 (2000) 1901.
17. R. Mishra and R. Balasubramaniam. *Corrosion Science*, 46 (2004) 3019.
18. Z. Szklarska-Smialowska. *Corrosion Science*, 41 (1999) 1743
19. G. S. Frankel. *Journal of the Electrochemical Society*, 145 (1998) 2186.
20. T.Charng and F.Lansing. *TDA Progress Report*, (1982) 42.
21. V. Shankar Rao. *Electrochimica Acta*, 49 (2004) 4533.
22. E.M. Esparza Zúñiga, M.A.Veloz Rodríguez, V.E. Reyes Cruz and J. Uruchurtu Chavarín, *Superficies y Vacío*, 25 (2012) 139.
23. C. Nelsy Raguá, J. Mónica Vera, Y. Darío and B. Peña, *Scientia et Technica*, 35 (2007) 213.
24. M. Zamanzade and A. Barnoush. *Corrosion Science*, 78 (2014) 223.

25. M. F. López, M. L. Escudero. *Electrochimica Acta* 43 (1998) 671.
26. N. De Cristofaro, S. Frangini and A. Mignone. *Corrosion Science*, 38 (1996) 307.
27. J. Ren and Y. Zuo. *Surface & Coatings Technology*, 191 (2005) 311.
28. S.N. Afzal, M.A. Ali Shaikh, C.M. Mustafa, M. Nabi, M.Q. Ehsan and A.H. Khan. *Journal of Nepal Chemical Society*, 22 (2007) 26.
29. D. Schaepers and H.H. Strehblow. *Corrosion Science*, 39 (1997) 2193.